Journal of Solid State Chemistry 182 (2009) 2991–2996

Contents lists available at ScienceDirect

Journal of Solid State Chemistry

journal homepage: www.elsevier.com/locate/jssc

Heterometallic clusters arising from cubic $Ni_3M'O_4$ (M' = K and Na) entity: Solvothermal synthesis with/without the assistance of microwave

Shu-Hua Zhang [a], Yan-Ling Zhou [a], Xiao-Jun Sun [b], Lian-Qiang Wei [a], Ming-Hua Zeng [a,*], Hong Liang [a,*]

[a] Key Laboratory for the Chemistry and Molecular Engineering of Medicinal Resources (Ministry of Education of China), School of Chemistry & Chemical Engineering of Guangxi Normal University, Guilin 541004, PR China

[b] College of Physics and Technology, Guangxi Normal University, Guilin 541004, PR China

ARTICLE INFO

Article history:
Received 27 June 2009
Received in revised form
5 August 2009
Accepted 7 August 2009
Available online 14 August 2009

Keywords:
Microwave
Solvothermal synthesis
Heterometallic cubic cluster
Magnetic properties

ABSTRACT

Solvothermal reaction assisted with microwave leads to the formation of two unique heterometallic cubic clusters $[Ni_3M'(L)_3(OH)(CH_3CN)_3]_2\cdots CH_3CN$ (M' = K for **1** and M' = Na for **2**, where L is an anion of 2-[(2-hydroxy-3-methoxy-benzylidene)-amino]-ethanesulfonate) with higher efficiency, yields and purity than those without it. The 6-metallacrown-3 $[Ni_3(OH)(L)_3]^-$ groups exhibit interesting ion trapping and self-assembly of size-different Na^+ and K^+ through form recognition and coordination activity in **1** and **2**. The magnetic studies for **1** and **2** suggest that the $\{Ni_3M'O_4\}$ (M' = K and Na) cores both display dominant ferromagnetic interactions from the nature of the binding modes of μ_3-O (oxidophenyl) and μ_3-OH.

1. Introduction

In the past decade, much attention has been given to the design and synthesis of polymetallic clusters since the discovery of "single-molecule magnets" (SMMs) [1–3]. The search for key ligands is an important process to advance this investigation. Recently, Schiff base, as old evergreen ligands, has been widely used in the synthesis of magnetic molecular clusters [4–6]. In particular, previous investigations have implied that metal complexes constructed by the sap^{2-} (sap^{2-} is the anion of 2-salicylide-neamino-1-propanolate) derivatives usually form cubane-based structures and probably favor ferromagnetic coupling through μ_3-O-bridges and towards SMM behavior. Herein, we chose one analogous ligand of 2-[(2-hydroxy-3-methoxy-benzylidene)-amino]-ethanesulfonate) to serve as chelating/bridging ligand to bring metal ions into new types of cubane-based clusters.

As is well known, the vast majority of paramagnetic cluster compounds are produced through the "conventional" technique, that is, mixing metal ion and ligand in a common solvent at temperatures limited by the boiling point of that solvent at atmospheric pressure. With the development of new preparative routes for the synthesis of molecular clusters under non-ambient conditions, several groups have explored high-temperature solvothermal methods to synthesize clusters [1–3,7]. Furthermore, very recently, microwave heating, as a new and extremely attractive method for obtaining polymetallic clusters, has been introduced into solvothermal synthesis and provides a clean, cheap and convenient way of heating, which can result in not only higher yields and shorter reaction time but also the formation of complete products [8–12]. An interesting aspect for synthetic inorganic chemists is exploring and widening new preparative routes under non-ambient conditions in different reaction systems. In our previous work [12], we have reported microwave-assisted synthesis for a disc-like, ferromagnetic heptanuclear Co(II) cluster, $[Co_7(immp)_6(MeO)_6]\cdots(ClO_4)_2$ (immp is 2-iminomethyl-6-methoxy-phenolic anion), and a heterometallic cubic Co(II) cluster, $[NaCo_3(L)_3(CH_3CN)_3\cdot(OH)]_2\cdot CH_3CN$. Here we demonstrate the solvothermal synthesis assisted with microwave vs without it of two new ferromagnetic heterometallic complexes $[Ni_3M'(L)_3(OH)(CH_3CN)_3]_2\cdot CH_3CN$ with $\{Ni_3M'O_4\}$ cubic cores.

2. Experimental

2.1. Materials

All chemicals were commercially available and used as received without further purification. M'_2L was prepared according to a literature procedure [13].

2.2. Synthesis

Preparation of ***1***: An acetonitrile solution (4 mL) of K_2L (0.335 g, 1 mmol) was added to an acetonitrile solution (4 mL) of

* Corresponding authors.
E-mail address: zmh@mailbox.gxnu.edu.cn (M.-H. Zeng).

0022-4596/$ - see front matter © 2009 Elsevier Inc. All rights reserved.
doi:10.1016/j.jssc.2009.08.009

$Ni(ClO_4)_2\cdots\cdot 6H_2O$ (0.360 g, 1 mmol). The mixture was stirred for 15 min and then 0.8 mL of triethylamine was added. The mixture was placed in a 15-mL Teflon-lined autoclave and heated at 140 °C for 1, 2, 3, 4, and 5 days, respectively. The autoclave was cooled over a period of 10 h at the rate of 10 °C h^{-1}, and **1** as green crystals were collected by filtration, washed with acetonitrile, and dried in air. Phase-pure crystals of **1** were obtained by manual separation. Yield: 19.9, 44.4, 79.7, 124.5, and 134.8 mg, respectively. Anal. calcd. (%) for $C_{74}H_{89}N_{13}K_2Ni_6O_{32}S_6$: C, 38.72; H, 3.91; N, 7.93; S, 8.36. Found: C, 38.66%; H, 4.12%; N, 8.01%; S, 8.33%. IR data for **1** (KBr, cm^{-1}): 3436(w), 2930(m), 1626(s), 1469(m), 1223(s), 1183(s), 1154(s), 1085(m), 1042(m), 761(w), 731(m), 519(w), 5497(w).

Preparation of ***2***: **2** can be prepared in a similar way as **1** except that K_2L was replaced by Na_2L. Phase-pure crystals of **2** were obtained by manual separation. Yield: 8, 19, 46, 72, and 77 mg, for 1, 2, 3, 4, and 5 days, respectively. Anal. calcd. (%) for $C_{74}H_{89}N_{13}Na_2Ni_6O_{32}S_6$: C, 39.27; H, 3.96; N, 8.04; S, 8.48; Found C, 39.12%; H, 4.15%; N, 7.97%; S, 8.41%. IR data for **2** (KBr, cm^{-1}): 3428(w), 2928(m), 1634(s), 1469(m), 1223(s), 1182(s), 1155(s), 1086(m), 1042(m), 762(w), 731(w), 519(w), 503(w).

At different times for 29, 58, 87, 116 and 145 min, respectively, complex **1** was also synthesized by microwave irradiation ($T = 140$ °C; power = 300 W; pressure = 8.1 atm), affording green crystals. Yield: 51.7, 85.8, 122.2, 148.2, and 161.3 mg, respectively. Anal. calcd. (%) for $C_{74}H_{89}N_{13}K_2Ni_6O_{32}S_6$: C, 38.72; H, 3.91; N, 7.93; S, 8.36; Found C, 38.62%; H, 4.06%; N, 8.02%; S, 8.38%. IR spectra contrast (Fig. S1) indicated that they are the same through two different synthesis methods.

Using microwave irradiation, **2** can be prepared in a similar way as that of **1** except that K_2L was replaced by Na_2L at the same condition. Yield: 10, 36, 74, 85, and 88 mg, respectively. Anal. calcd. (%) for $C_{74}H_{89}N_{13}Na_2Ni_6O_{32}S_6$: C, 39.18; H, 4.09; N, 8.03; S, 8.47; Found C, 39.14%; H, 4.18%; N, 7.98%; S, 8.43%. IR (Fig. S2) spectra of the products indicate that they are also the same through two different synthesis methods, as well as PXRD spectra of the compounds identify phase purity of the bulk samples synthesized by different ways (Fig. S3).

2.3. Physical measurements

C, H, and N microanalyses were carried out with an Elemental Vario-EL CHNS elemental analyzer. FT-IR spectra were recorded from KBr pellets in the range 4000–400 cm^{-1} on a Bio-Rad FTS-7 spectrometer. Powder diffraction was carried out by Rigaku D/max 2500v/pc diffraction. Magnetic susceptibility measurements were performed on a polycrystalline sample fixed on a Quantum Design MPMS-XL5 SQUID for **1** and MPMS-XL7 SQUID for **2**.

2.4. Crystallography

Single crystal X-ray diffraction analyses of the two compounds were carried out on a Bruker SMART APEX CCD diffractometer equipped with a graphite monochromated Mo $K\alpha$ radiation ($\lambda = 0.71073$ Å) by using the $\omega-\theta$ scan technique at 293 K. Raw frame data were integrated with the SAINT program [14]. The structures were solved by direct methods with SHELXS-97 and refined by full-matrix least-squares on F^2 using SHELXS-97 [14]. The empirical absorption correction was applied with the program SADABS [14c]. All non-hydrogen atoms were refined anisotropically. The hydrogen atoms were set in the calculated positions and refined by a riding mode. The anisotropic displacement parameters of O6, C10, C13, C14, N3 and N3′ in **1** and **2** were restrained to be identical with a standard uncertainty of 0.01 $Å^2$ for terminal atoms. C13 and C13′, N3 and N3′, C14 and C14′ atoms have been restrained by the same displacement parameter for **1** and **2**. The crystallographic details are provided in Table 2, while the selected bond distances and angles are listed in Table 3. Crystallographic data for the structural analysis have been deposited with the Cambridge Crystallographic Data Center. CCDC reference numbers for **1** and **2** are 698153 and 659671.

3. Results and discussion

3.1. Synthesis

For **1**, using the solvothermal method, after 1 day, the products appear with small clarity crystals and concomitancy mass green power (Fig. S4 and Table 1). With a long time from 2 to 5 days, the quantity of the green powder diminishes, concomitant with an increase in the yield and size, and decrease in transparency of the crystals with a final yield of 35.2%.

For **2**, after 1 day, the products also appear with very small clarity crystals and concomitancy mass green power (Fig. 1 and Table 1). With a long time from 2 to 4 days, the quantity of the green powder diminishes, concomitant with an increase in the yield, size and transparency of the crystals. Through 5 days of crystallization processing, the size of the crystals continuingly with a final yield of 20.4%, but most of the crystals are not suitable for single crystal X-ray analysis.

With a parallel comparison, the experiment is assisted with microwave irradiation under the same temperature condition. For **1**, after only 29 min, the small products are formed with opacity, small coarse crystals and most of them are not suitable for single crystal X-ray analysis. Increasing the reaction time from 58 to 145 min, the average size of crystals increases from 0.4 to 2.3 mm along with good quality, and the yield increases from 22.4% to 42.1%, respectively.

For **2**, the experimental phenomena are the same as that of **1**, but after 145 min of crystallization period, we gain the biggest size crystals with the final yield of 23.3%, and also lose the quality of crystals for single crystal X-ray analysis (Fig. 1).

We found that with an increase in the reaction time under the two different methods, the heteromorphism becomes more obvious under microwave irradiation than without it, because of their obviously different growth rates.

Presenting a striking contrast to assist with microwave irradiation, the quality and yield of product are obviously better than using common solvothermal methods, with shortened reaction time [5].

3.2. Crystal structures

The two compounds are practically identical (Table 2), differing by the nature of the alkali ions (K^+ (**1**) and Na^+ (**2**)), and their crystal structures will be described simultaneously and referred as {$NaNi_3$}. Compound **2** crystallizes in the trigonal space group $R\bar{3}$, and its structure consists of a heterometallic cubic

Table 1
Relation yield and time for **1** and **2**.

1	Microwave	Time (min)	29	58	87	116	145
		Yield (%)	13.5	22.4	31.9	38.7	42.1
	Without microwave	Time (day)	1	2	3	4	5
		Yield (%)	5.2	11.6	20.8	32.5	35.2
2	Microwave	Time (min)	29	58	87	116	145
		Yield (%)	2.7	9.5	19.6	22.5	23.3
	Without microwave	Time (day)	1	2	3	4	5
		Yield (%)	2.1	5.0	12.2	19.10	20.4

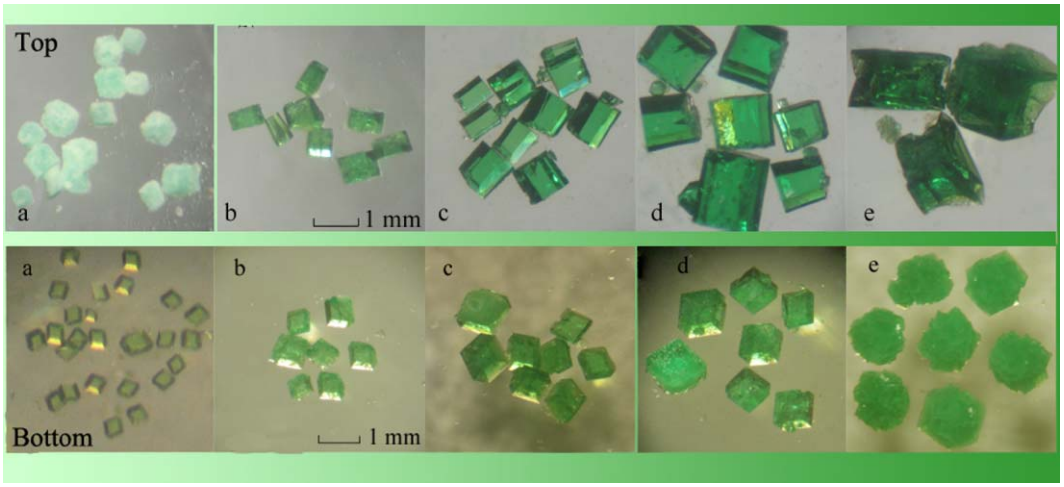

Fig. 1. The series of part crystal photos with different reaction times for **2**: top, assisted with microwave: (a) 29 min, (b) 58 min, (c) 87 min, (d) 116 min, and (e) 145 min; bottom, accustomed solvothermal: (a) 1 , (b) 2, (c) 3, (d) 4, and (e) 5 days.

Table 2
Crystal data and structure refinement for **1** and **2**.

Compound	**1**	**2**
Fw	2295.34	2263.12
T(K)	293(2)	293(2)
Crystal system	Trigonal	Trigonal
Space group	$R\bar{3}$	$R\bar{3}$
a (Å)	16.884(1)	16.984(1)
b (Å)	16.884(1)	16.984(1)
c (Å)	27.617(4)	27.192(1)
V (Å^3)	6818.3(1)	6792.7(6)
Z	3	3
D_{calcd} (g cm^{-3})	1.679	1.660
μ (mm^{-1})	1.536	1.459
GOF	1.036	1.049
R_1 [$I \geq 2\sigma(I)$][a,b]	0.0607	0.0344
wR_2 (all data)[a,b]	0.1939	0.0941
Residues/e Å^{-3}	0.734 and -0.603	0.987 and -0.293

[a] $R_1 = \sum||F_o|-|F_c||/\sum|F_o|$.
[b] $wR_2 = [\sum w(F_o^2-F_c^2)^2/\sum w(F_o^2)^2]^{1/2}$.

cluster [15], with organic moieties and free guest acetonitrile molecules stretching out of the cluster. An alternative view of the host compound along its virtual C_3 axis is presented in Fig. 2a (Na atom is not presented here for clarity). The nickel atoms lie at the vertices of an equilateral triangle through a μ_3-OH bridge, with the nickel–nickel separations being equal within experimental error. In comparison, the nickel–nickel separation [3.128(1) Å] in **2** is 0.672 Å, which is shorter than the previously reported trinuclear Ni(II)-complex $[Ni_3(N_3)_3(O_2CMe)_3(py)_5]$ [9]. The *O*, *N*, *O*-chelating sites from L^{2-}, one μ_3-OH$^-$ group and one terminal acetonitrile ligand complete the octahedral coordination sphere of each nickel atom, while the L^{2-} anions exhibit an unusual hexadentate μ_3:η^1:η^3:η^1:η^1 coordination mode in the cluster, which is different from the *O*, *N*-chelating mode of its reported single-schiff base compounds. The $[Ni_3(OH)(L)_3]^-$ core described so far approaches the C_3 point symmetry and small differences are found in the bond distances of each nickel center with oxygen atoms from the peripheral L ligands. Namely, Ni1–O4A [2.115(2) Å] is longer than Ni1–O4 [2.032(2) Å] on careful inspection of the metrical parameters. The Ni1–O6(μ_3-OH)–Ni1A angle is 99.8(1)° and the Ni1–O4–Ni1A angle is 97.9(1)°, with all the angles less than 100°, are in the range for Ni···Ni ferromagnetic exchange pathways to be dominant from 90° to 104° [16,17].

A fascinating and peculiar feature of **2** is the complex core, $[Ni_3O_3(OH)]^-$, displaying a 6-metallacrown-3 structure and acting as a host for an alkali-metal ion, which has a trigonally distorted octahedral environment. The nickel–oxygen core of complex **2** is an excellent ion-trapping hemi-cavity in which the six-membered ring of nickel and oxygen atoms Ni1–O4–Ni1B–O4B–Ni1A–O4A acts as a groove, while the methoxy groups from three different *L* act as buckles upside. As shown in Fig. 2b and c, the residual six proper coordination atoms on the templating cavity act as alkali ion (Na^+ and K^+) trapping sites. All the above observations can be satisfactorily rationalized by considering the arrangement of the Na ion and three methoxy groups from different *L* ligands, with respect to the 6-metallacrown of the $[Ni_3Na(L)_3(OH)(CH_3CN)_3]^-$ core. The nickel centers and the sodium ions in **2** are found at the vertices of a distorted tetrahedron, whose metrical parameters are summarized in Table 3. The sodium ion occupies the molecular hemi-cavity, which results from the arrangement of the nickel–oxygen framework of the trinuclear core and is coordinated by the three methoxy group donors from three different *L*. The Na^+ ion forms $[NaO_6]$ octahedral geometry completed by three *O*, *O*-chelating sites from phenolato oxygen and methoxy groups of three different L^{2-} [18–20]. The Na–O bonds ranging from 2.318(2) to 2.398(2) Å are markedly narrower than those of crown ether (Na–O distances range from 2.234(1) to 2.410(1) Å) [21–23]. Therefore, the L^{2-} ligand as hetero-multinucleating ligands can incorporate one "soft" (Ni^{2+}) metal center and one "hard" (Na^+) metal center (Scheme 1). The $\{Ni_3NaO_4\}$ cubic cluster is distorted from the S_4 symmetry to C_3, resulting from the difference in the ion radius between nickel and sodium. In particular, the μ_3-O (phenolato) coordination model of the L^{2-} anion is singular [14,21,22,24]. It is somewhat surprising that very limited heterometallic oxacubane structures have been reported. Such 6-metallacrown-3 mixed alkaline metal quarters compounds are known for Zn, Tc, Mo, Cr, and Fe [1,2,25–29]. The presence of a Ni_3NaO_4 core in **2** is unprecedented in contrast to the well-documented tetranuclear cubane-type molecular structures [1–3,14]. In the present case, size-different Na^+ and K^+ (Fig. S5) may seem to share the basic attractive power of form recognition and coordination activity of 6-metallacrown-3 $[Ni_3(OH)(L)_3]^-$ SBU, which governs the process of ion trapping and self-assembly in compounds **1** and **2**.

There is no significant intercluster interaction except very weak O–H···N (O6–H6B···N3′, 3.223(13) Å, 180°) hydrogen bonds (Fig. S6). The centroid–centroid distance of adjacent clusters is 10.8(1) Å. A space-filling plot of **2** reveals that the cluster has

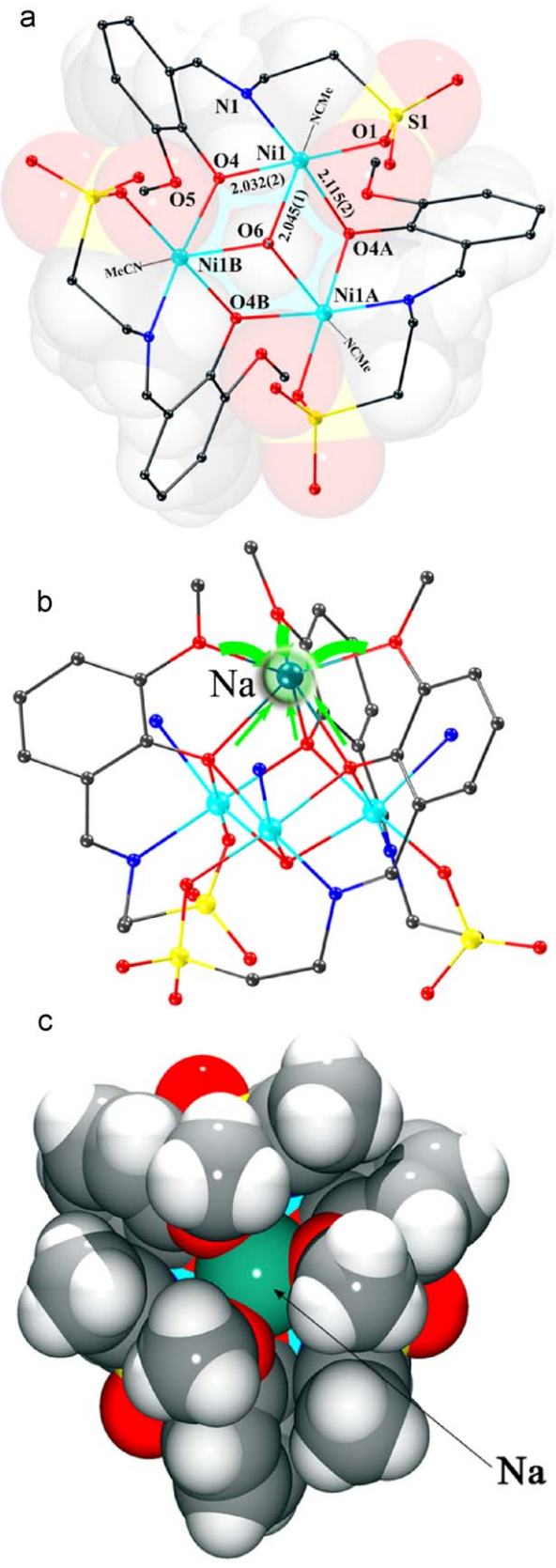

Fig. 2. Bottom views of coordination geometries of nickel(II) atoms in **2** (some equivalent atoms are generated to complete the Ni coordination, solvent molecules, H atom omitted), (a) side view (Na^+ is not presented here for clarity), (b) top view of **2**, and (c) space filling view of **2**. Colors: carbon, gray; hydrogen, white; oxygen, red; nitrogen, blue; nickel, cyan. (For interpretation of references to colour in this figure legend, the reader is referred to the web version of this article.)

Table 3
Selected bond distances (Å) and angles (°).

Compound[a]	1	2
Ni1–O1	2.041(4)	2.032(2)
Ni–O6	2.047(3)	2.045(1)
Ni1–O4	2.033(4)	2.032(2)
Ni1–N1	2.047(5)	2.037(2)
Ni1–N2	2.114(6)	2.152(2)
Ni1–O4a	2.131(4)	2.115(2)
M′–O4	2.325(5)	2.318(2)
M′–O5	2.393(6)	2.398(2)
Ni···Ni	3.125(1)	3.128(1)
Ni···M′	3.321(1)	3.302(2)
O4a–M′–O4	76.0(2)	76.2(1)
O4–M′–O5	67.7(2)	67.8(1)
O4a–M′–O5b	111.1(2)	111.7(1)
O4b–M′–O5	139.3(2)	139.1(1)
O5b–M′–O5	108.4(2)	108.1(1)
O4–Ni1–O1	176.3(2)	176.1(1)
O4–Ni1–O6	82.4(2)	81.8(1)
O1–Ni1–O6	100.0(2)	100.8(1)
O4–Ni1–N1	89.1(2)	89.0(1)
O1–Ni1–N1	93.3(2)	93.6(1)
O6–Ni1–N1	97.5(2)	97.5(1)
O4–Ni1–N2	89.3(2)	86.7(1)
O1–Ni1–N2	87.9(2)	90.3(1)
O6–Ni1–N2	168.1(2)	165.7(1)
N1–Ni1–N2	90.9(2)	90.6(1)
O4a–Ni1–O4	86.9(2)	87.2(1)
O1a–Ni1–O4	90.8(2)	90.4(1)
O6a–Ni1–O4	80.1(2)	79.8(1)
N1a–Ni1–O4	175.5(2)	175.6(1)
N2a–Ni1–O4	91.0(2)	91.3(1)
Ni1a–O6–Ni1	99.5(2)	99.8(1)
Ni1b–O4–Ni1	97.2(2)	97.9(1)

[a] Symmetry codes: a: 1−*y*, *x*−*y*, *z*; b: 1−*x*+*y*, 1−*x*, *z*.

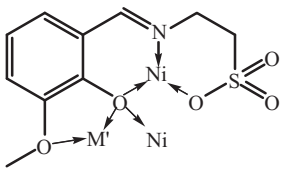

Scheme 1. Coordination mode of the L^{2-} (M' = K for **1** and M' = Na for **2**).

an approximate trefoil shape with a diameter of ca. 12.67(1) Å (Fig. S7).

For **1** and **2**, the Ni···Ni distances increase from 3.125 to 3.131 Å, while Ni···M' distances shorten from 3.319 to 3.290 Å, when the M' ions changed from K^+ to Na^+ (Table 3).

3.3. Magnetic studies

The magnetic data were measured on crushed single crystals. The dc magnetization data of **1** and **2** are shown in Fig. 3. The values of $\chi_m T$ at 300 K are ca. 4.38 and 4.34 $cm^3\,K\,mol^{-1}$ for **1** and **2**, respectively, being slightly highter than the spin-only value of 3 $cm^3\,K\,mol^{-1}$ assuming $g = 2.0$, and almost equal to the value of $\chi_m T$ at 300 K of $[Ni_3(N_3)_3(O_2CMe)_3(py)_5]$ [9]. As T decreases, the $\chi_m T$ smoothly increases to 5.49 $cm^3\,K\,mol^{-1}$ for **1** and to 5.38 $cm^3\,K\,mol^{-1}$ for **2** at ca. 45 K, while upon further decrease in T, it rapidly increases to a maximum of 7.36 $cm^3\,K\,mol^{-1}$ for **1** and to 6.96 $cm^3\,K\,mol^{-1}$ for **2** at 9 K, and then smoothly decreases to 6.27 $cm^3\,K\,mol^{-1}$ for **1** and to 6.03 $cm^3\,K\,mol^{-1}$ for **2** at 2 K.

The temperature dependence of the reciprocal susceptibility (χ_m^{-1}) above 50 K follows the Curie–Weiss law ($\chi_m = C/(T-\theta)$) with a Weiss constant of $\theta = 3.97$ K and a Curie constant of $C = 4.21$

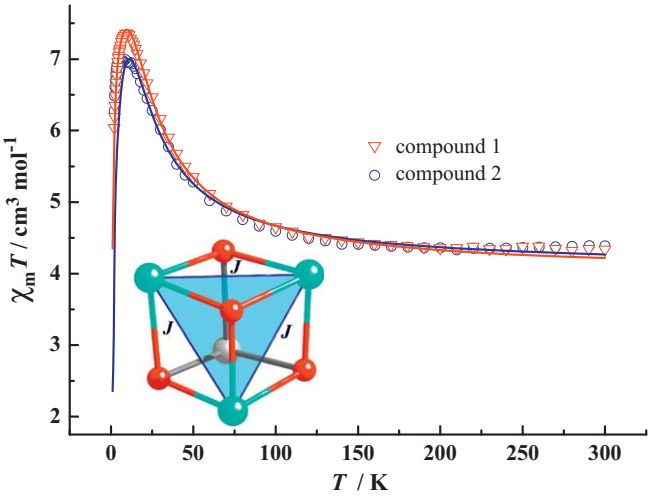

Fig. 3. Plot of $\chi_m T$ vs T for (a) **1** and (b) **2**; the solid line represents the fit of data in the temperature range. (inset: the exchange pathway between the Ni(II) ions).

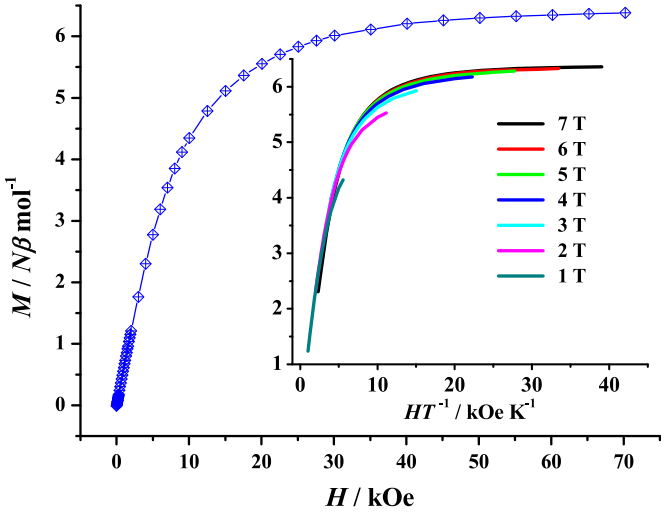

Fig. 4. Field dependence of magnetization for **2** at 1.8 K. Inset are the isofield lines of reduced magnetization ($M/N\beta$) vs H/T.

cm^{-1} K mol^{-1} for **1,** and $\theta = 14.89$ K and $C = 3.69$ cm^{-1} K mol^{-1} for **2** (Fig. S8). The larger positive Weiss constant indicates a dominated intramolecular ferromagnetic interaction between the adjacent Ni(II) ions through the two kinds of oxygen atom exchange bridges. The low-temperature maximum indicates an $S = 3$ ground state (with $g = 2.17$). This pattern is compatible with moderate ferromagnetic coupling [8–12,18–20], and the sudden decrease in $\chi_m T$ at low temperature is assigned to either zero-field splitting within the ground state or intermolecular antiferromagnetic interactions.

The analysis of field-dependent magnetic data collected in strong (1–7 T) magnetic fields at temperatures ranging from 1.8 to 10.0 K was attempted in order to garner additional information on the magnetic behavior of **2** (Fig. 4). The plots of reduced magnetization M vs H/T suggest that there is no obviously big zero-field splitting in **2** because the isofield lines are not entirely separated, as shown in the inset of Fig. 4. At high field (>2 T), the moments obviously towards saturated value. The situation present in **2** is fundamentally different from that encountered in the nickel-based established SMMs, and the curves could not be well fitted by the ANISOFIT method [18–20].

The ac measurements in the range 10–997 Hz for **1** and 1–1500 Hz for **2** were checked. Both no frequency dependence of the in-of-phase ac signals and no out-of-phase ac signals reveal none of the slow relaxation effects (Fig. S9) above 1.8 K, and confirm the above analysis of field dependence of the magnetization, indicating that **1** and **2** do not behave as an SMM.

An examination of the bond lengths and angles between the Ni(II) centers in **1** and **2** for magneto-structural correlations reveals an obvious trend based on the structural parameters. When the values reported for the different Ni(II) clusters are compared, some general observations can be made. Three intracubic Ni···Ni interactions (J, Inset Fig. 3) are nearly equilateral because of the molecule possession along the C_3 axis (M'···O6), with the range from 97.6° to 99.5° for **1** and from 97.9° to 99.8° for **2**, tending to yield orthogonality for Ni···Ni ferromagnetic superexchange pathways [30]. Employing the anisotropic spin Hamiltonian in Eq. (1) and χ_m in Eq. (2) allows us to satisfactorily model the data with the parameters $J = +4.33$ cm^{-1}, $D = 0.66$ cm^{-1}, and $g = 2.31$ for **1** and $J = +4.45$ cm^{-1}, $D = 0.51$ cm^{-1}, and $g = 2.27$ for **2** (Fig. 3).

$$\hat{H} = -2J(\hat{S}_1\hat{S}_2 + \hat{S}_1\hat{S}_3 + \hat{S}_2\hat{S}_3) + D\sum_{i=1}^{3}\hat{S}_{iz} \quad (1)$$

$$\chi_m = \frac{2N_A\mu_B^2}{kT}\frac{g^2}{}\frac{F_1}{F_2} \quad (2)$$

$$\begin{aligned} F_1 = {} & 8\exp\{D/kT\} \\ & + 9\exp\{6J/kT\} \\ & + 4\exp\{(D+6J)/kT\} + 2\exp\{(D-2J-\sqrt{D^2+4J^2})/kT\} \\ & + 2\exp\{(D-2J+\sqrt{D^2+4J^2})/kT\} \\ & + \exp\{(D+J-\sqrt{D^2+6DJ+25J^2})/kT\} \\ & + \exp\{(D+J+\sqrt{D^2+6DJ+25J^2})/kT\} \end{aligned}$$

$$\begin{aligned} F_2 = {} & 6\exp\{D/kT\} \\ & + \exp\{(D-6J)/kT\} \\ & + 2\exp\{(D-4J)/kT\} \\ & + 2\exp\{6J/kT\} \\ & + 2\exp\{(D+6J)/kT\} + 4\exp\{(D-2J-\sqrt{D^2+4J^2})/kT\} \\ & + 4\exp\{(D-2J+\sqrt{D^2+4J^2})/kT\} \\ & + \exp\{(2D+J-\sqrt{D^2-2DJ+25J^2})/kT\} \\ & + \exp\{(2D+J+\sqrt{D^2-2DJ+25J^2})/kT\} \\ & + 2\exp\{(D+J-\sqrt{D^2+6DJ+25J^2})/kT\} \\ & + 2\exp\{(D+J+\sqrt{D^2+6DJ+25J^2})/kT\} \end{aligned}$$

On the other hand, a complete analysis of the magnetic exchange interactions has been performed by means of the full-matrix diagonalization program MAGPACK [31], applying the anisotropic Hamiltonian in Eq. (1). The best-fit parameters obtained with this computing model are the same as the above results. The values of exchange-parameter in the two above models are comparable to those previously reported Ni(II) complexes with similar bridges in Ni_4O_4 cubic cores with the range from 3.65 to 6.55 cm^{-1} [1,32]. Furthermore, almost similar values of exchange parameters for **1** and **2** indicate the different alkali-metal ions play an unconspicuous effect for the magnetic properties of such clusters. However, Cornia et al. have reported two antiferromagnetic iron(III) rings $[LiFe_6(OMe)_{12}(dbm)_6]$ and $[NaFe_6(OMe)_{12}(pmdbm)_6]$, where Hdbm = 1,3-diphenyl-1,3-propanedione and Hpmdbm = 1,3-di(4-methoxyphenyl)-1,3-propanedione, in which Li^+ and Na^+ tune well

the magnetic properties of SMMs. The sign of the D parameter in the best fit is positive and attempting to fit the susceptibility data with negatives values of D is not proper. The value of $D>0$ is in agreement with the absence of SMM properties of **1** and **2** [33].

4. Conclusions

In conclusion, the combination of nickel and alkali-metal ions, as well as a special schiff base ligand L^{2-}, is a good strategy for obtaining novel "heterometallic cubane-like" systems. Our result assisted with microwave parallelly in comparison with accustomed solvothermal methods to form the ferromagnetic $\{Ni_3M'O_4\}$ clusters, highlights that microwave irradiation provides a new, fast and powerful synthetic tool to acquire new polymetallic complexes during the solvothermal synthesis process. Magnetic measurements show that the $Ni_3M'O_4$ ($M'=$ K and Na) cubes are not an SMM, probably resulting from the positive value of D and the minimum intermolecular interactions.

Acknowledgments

This work was supported by NSFC (No. 20871034), the Program for New Century Excellent Talents in University of the Ministry of Education China (NCET-07-217), the Project of Ten, Hundred, Thousand Distinguished Talents in New Century of Guangxi (No. 2006201) and Fok Ying Tung Education Foundation (111014), as well as GKN (Grant 0630006-5D).

Supplementary material

CCDC 698153 and 659671 contain the supplementary crystallographic data for this paper. Copies of the data can be obtained free of charge via the Internet at http://www.ccdc.cam.ac.uk/conts/retrieving.html or by post at CCDC, 12 Union Road, Cambridge CB2 1EZ, UK (Fax: +44 1223336033, Email: deposit@ccdc.cam.ac.uk). The series of part crystal photos for **1**. Perspective views of the crystal packing in **2**; Space-filling plot of **2**; χ_m^{-1} vs. T curve; Field dependence of magnetization for **1** at 2 K; IR curves, XRD and theory simulation curves.

Appendix A. Supplementary materials

Supplementary data associated with this article can be found in the online version at doi:10.1016/j.jssc.2009.08.009

References

[1] M. Fujita, A. Powell, C. Creutz (Eds.), From the Molecular to the Nanoscale: Synthesis, Structure, and Properties, Vol. 7, Elsevier, Oxford, 2004.
[2] D. Gatteschi, R. Sessoli, Angew. Chem. Int. Ed. 42 (2003) 268–297.
[3] M.H. Zeng, M.X. Yao, H. Liang, W.X. Zhang, X.M. Chen, Angew. Chem. Int. Ed. 46 (2007) 1832–1835.
[4] H. Oshio, N. Hoshino, T. Ito, M. Nakano, J. Am. Chem. Soc. 126 (2004) 8805–8806;
H. Oshio, M. Nihei, S. Koizumi, T. Shiga, H. Nojiri, M. Nakano, N. Shirakawa, M. Akatsu, J. Am. Chem. Soc. (2005) 4568–4569;
S. Koizumi, M. Nihei, T. Shiga, M. Nakano, H. Nojiri, R. Bircher, O. Waldmann, S.T. Ochsenbein, H.U. Güdel, F. Fernandez-Alonso, H. Oshio, Chem. Eur. J. (2007) 8445–8453.
[5] T.C. Stamatatos, D. Foguet-Albiol, S.-C. Lee, C.C. Stoumpos, C.P. Raptopoulou, A. Terzis, W. Wernsdorfer, S.O. Hill, S.P. Perlepes, G. Christou, J. Am. Chem. Soc. 129 (2007) 9484–9499.
[6] C.J. Milios, R. Inglis, A. Vinslava, R. Bagai, W. Wernsdorfer, S. Parsons, S.P. Perlepes, G. Christou, E.K. Brechin, J. Am. Chem. Soc. 129 (2007) 12505–12511.
[7] R.H. Laye, E.J.L. McInnes, Eur. J. Inorg. Chem. (2004) 2811–2818.
[8] C.J. Millos, A.G. Whittaker, E.K. Brechin, Polyhedron 26 (2007) 1927–1933 and the references therein.
[9] C.J. Milios, A. Prescimone, J. Sanchez-Benitez, S. Parsons, M. Murrie, E.K. Brechin, Inorg. Chem. 45 (2006) 7053–7055.
[10] C.J. Milios, A. Vinslava, A.G. Whittaker, S. Parsons, W. Wernsdorfer, G. Christou, S.P. Perlepes, E.K. Brechin, Inorg. Chem. 45 (2006) 5272–5274.
[11] I.A. Gass, C.J. Milios, A.G. Whittaker, F.P.A. Fabiani, S. Parsons, M. Murrie, S.P. Perlepes, E.K. Brechin, Inorg. Chem. 45 (2006) 5281–5283.
[12] S.H. Zhang, S. You, H. Liang, M.H. Zeng, Cryst. Eng. Comm. 11 (2009) 865–872.
[13] S.H. Zhang, Y.M. Jiang, Z.Y. Zhou, Chin. J. Chem. 22 (2004) 1303–1307.
[14] Siemens, SAINT: Area Detector Control and Integration Software, Siemens Analytiacl X-ray instruments Inc., Madison, WI, USA, 1996;
G.M. Sheldrick, SHELXL97 and SHELXTL Software Reference Manual, Version 5.1, Brucker AXS Inc., Madison, WI, USA, 1997;
G.M. Sheldrick, SADABS. Program for Empirical Absorption Correction of Area Detector Data,, University of Göttingen, Germany, 1996.
[15] S. Deeken, S. Proch, E. Casini, H.F. Braun, C. Mechtler, C. Marschner, G. Motz, R. Kempe, Inorg. Chem. 45 (2006) 1871;
R. Hernández-Molina, I.V. Kalinina, P.A. Abramov, M.N. Sokolov, A.V. Virovets, J.G. Platas, R. Llusar, V. Polo, C. Vicent, V.P. Fedin, Inorg. Chem. (2008) 306–314.
[16] M.L. Tong, M. Monfort, J.M.C. Juan, X.-M. Chen, X.-H. Bu, M. Ohba, S. Kitagawa, Chem. Commun. (2005) 233–235.
[17] B. Cage, F.A. Cotton, N.S. Dalal, E.A. Hillard, B. Rakvin, C.M. Ramsey, J. Am. Chem. Soc. 125 (2003) 5270–5271.
[18] J. Martin-Frtre, Y. Jeannin, F. Robert, J. Vaissermann, Inorg. Chem. 30 (1991) 3635–3639.
[19] P.V. Bernhardt, E.J. Hayes, Inorg. Chem. 41 (2002) 2892–2902.
[20] M. Kemmer, M. Biesemans, M. Gielen, J.C. Martins, V. Gramlich, R. Willem, Chem. Eur. J. 7 (2001) 4686–4695.
[21] P. Even, B. Boitrel, Coord. Chem. Rev. 250 (2006) 519–541.
[22] S. Yamada, Coord. Chem. Rev. 190 (1999) 537–555.
[23] W.A. Herrmann, R. Alberto, J.C. Bryan, A.P. Sattelberger, Chem. Ber. 124 (1991) 1107–1111.
[24] P. Sobota, M. Klimowicz, J. Utko, L.B. Jerzykiewicz, New J. Chem. 24 (2000) 523–526.
[25] A.D. Bond, D.J. Linton, P. Schooler, A.E.H. Wheatley, J. Chem. Soc. Dalton Trans. (2001) 3173–3178.
[26] K. Merz, S. Block, R. Schönen, M. Driess, Dalton Trans. (2003) 3365–3369.
[27] A. Johansson, V.G. Kessler, Polyhedron 19 (2000) 1791–1798.
[28] J.J.H. Edema, S. Gambarotta, W.J.J. Smeets, A.L. Spek, Inorg. Chem. 30 (1991) 1380–1384.
[29] A. Caneschi, A. Cornia, A.C. Fabretti, D. Gatteschi, W. Malavasi, Inorg. Chem. 34 (1995) 4660–4668.
[30] K.K. Nanda, L.K. Thompson, J.N. Bridson, K. Nag, J. Chem. Soc. Chem. Commun. (1994) 1337–1338 and the references therein.
[31] J.J. Borrás-Almenar, J.M. Clemente-Juan, E. Coronado, B. Tsukerblat, Inorg. Chem. 38 (1999) 6081–6088;
J.J. Borrás-Almenar, J.M. Clemente-Juan, E. Coronado, B. Tsukerblat, J. Comput. Chem. (2001) 985–991.
[32] E.C. Yang, W. Wernsdorfer, L.N. Zakharov, Y. Karaki, A. Yamaguchi, R.M. Isidro, G.D. Lu, S.A. Wilson, A.L. Rheingold, H. Ishimoto, D.N. Hendrickson, Inorg. Chem. 45 (2006) 529.
[33] A. Cornia, M. Affronte, A.G.M. Jansen, G.L. Abbati, D. Gatteschi, Angew. Chem. Int. Ed. 38 (1999) 2264–2266.